 doi:10.20944/preprints202210.0335.v1

Article

Sustainable Synthesis of Sulfur-Single Walled Carbon Nanohorns Composite for Long Cycle Life Lithium-Sulfur Battery

Eleonora Venezia [1,2], Pejman Salimi [1,2], Susana Chauque [1], Remo Proietti Zaccaria [1,3,*]

[1] Istituto Italiano di Tecnologia, via Morego 30, Genova 16163, Italy; eleonora.venezia@iit.it, pejman.salimi@iit.it, susana.chauque@iit.it, remo.proietti@iit.it
[2] Department of Chemistry and Industrial Chemistry, University of Genova, via Dodecaneso 31, I-16146 Genova, Italy; eleonora.venezia@iit.it, pejman.salimi@iit.it
[3] Department of Physics, Shaoxing University, Shaoxing 312000, China; remo.proietti@iit.it
* Correspondence: remo.proietti@iit.it; Tel.: +39 331 2576045

Abstract: The preparation of sulfur-single walled carbon nanohorns active material via a simple and sustainable evaporation method for application as cathode in lithium-sulfur batteries is reported. We show that the synthesis process enables the infiltration of elemental sulfur within the carbon nanohorns thus obtaining a morphology responsible for the ameliorating of the shuttle effect. The sulfur-carbon composite is characterized in terms of structure, morphology, and composition through x-ray diffraction, transmission electron microscopy, and thermogravimetric analyses. From the electrochemical point of view, cyclic voltammetry, rate capability, and galvanostatic cycling tests are performed employing a solution of bis(trifluoromethane)sulfonimide lithium salt and lithium nitrate in a mixture of 1,2-dimethoxyethane and 1,3-dioxolane in order to evaluate the electrode design applicability within lithium-sulfur cells. In this respect, further insights are provided by the estimation of the lithium-ion diffusion coefficient through the Randles-Sevcik equation, and by electrochemical impedance spectroscopy. The obtained results reveal a remarkable cycle life lasting around 800 cycles with a stable capacity of 520 mA h g^{-1} for the first 400 cycles at C/4, while reaching a value around 300 mA h g^{-1} at the 750th cycle. These results suggest sulfur-carbon nanohorns active material as a potential candidate for the next-generation battery technology.

Keywords: lithium-sulfur batteries, single-walled carbon nanohorns, long cycle life, sustainable synthesis process

1. Introduction

The recent technological advancements in the electric mobility field, portable electronics and smart energy grids have been driving the scientific community working in the energy storage field towards the development and employment of higher energy density as well as more environmental friendly materials.[1,2] Indeed, the commercially available lithium-ion batteries (LIBs) are unable to meet these requirements due to their intrinsic limited energy density, thus new kinds of battery technologies need to be developed.[3,4] As a result, the next-generation of energy storage systems, such as lithium-air, lithium-sulfur and sodium-ion batteries are currently under deep investigation.[5,6] In particular, lithium-sulfur batteries (LSBs) which employ elemental sulfur as cathode active material, are widely investigated as a convincing alternative to LIBs.[7] Their electrochemical redox reaction involves the conversion of elemental sulfur S_8 to lithium sulfide Li_2S,[8,9] thus resulting in a remarkable theoretical capacity of 1675 mAh g^{-1} and an energy density as high as 2600 Wh kg^{-1}.[10,11] Additional benefits of using sulfur as active material are its non-toxicity, wide availability and low cost.[12]

On the other hand, it is well-known that lithium-sulfur cells suffer for three main issues, namely the low conductivity of sulfur and lithium sulfide, the lithium polysulfide (LiPSs) dissolution within organic electrolyte with the associated shuttle effect, and the

Preprints (www.preprints.org) | NOT PEER-REVIEWED | Posted: 21 October 2022 doi:10.20944/preprints202210.0335.v1

volume expansion of sulfur particles upon cycling.[13–16] In order to solve the aforementioned drawbacks various strategies have been introduced, such as tailoring the electrolyte composition, the application of metal oxides particles within the cathode and the insertion of functional interlayers.[17–22] All these approaches, although effective in enhancing the electrochemical performance of LSBs, require additional steps in the active material synthesis or in the cell assembly, thus resulting in an increase cell cost and augmented time-consuming production processes. Another well-explored technique capable of improving the LSBs performance is combing elemental sulfur with different kinds of host materials, mainly based on carbon, such as multi-walled carbon nanotubes, graphene, and mesoporous carbon.[23–27] These carbonaceous matrixes are capable of not only increasing the active material conductivity and reducing the detrimental effect related to the sulfur volumetric expansion, but they are also able to confine or retain the polysulfides species thus leading to an improved cycling stability.[28–30] Furthermore, the associated synthesis of the composite active material typically involves solvothermal or melting processes for whom only one production step is needed.[31,32]

With the aim of reducing the production costs and the synthesis steps, in this work we investigate the use of single-walled carbon nanohorns (SWCNHs) as possible sulfur host material through the implementation of a straightforward and sustainable evaporation method. SWCNHs are a class of material belonging to the fullerene family[33] and they are composed by graphitic tubules showing a peculiar horn-shape. These tubules, upon aggregation, form different spherical structures, namely dahlia-like, seed-like and bud-like structures.[34] They exhibit a good electrical conductivity, a large surface area and high pore volume.[35] Moreover, SWCNHs can be mass-produced by arc-discharge and CO_2 laser evaporation techniques.[36,37] Few papers report the use of SWCNHs in the battery field,[38–40] while they have been widely studied for biosensing, drug-delivery applications, gas storage and catalysis.[41–44] As anticipated, the active material herein described was obtained through an easy and sustainable solvent evaporation method enabling the direct infiltration of elemental sulfur within the carbonaceous matrix. The electrochemical performance of the designed electrode was tested in LSBs configuration by using a solution of bis(trifluoromethane)sulfonimide lithium salt and lithium nitrate in a mixture of 1,2-dimethoxyethane and 1,3-dioxolane. The results show a remarkable long cycle life of about 800 cycles at C/4 showing a capacity of 520 mA h g^{-1}, value that decreases down to about 300 mA h g^{-1} at the end of the cell life. This behaviour could arise from the physical retention of the LiPSs species within the SWCNHs.

2. Materials and Methods

2.1 Electrolyte preparation

The electrolyte solution was prepared by dissolving 1 mol kg^{-1} of bis(trifluoromethane)sulfonimide lithium salt (LiTFSI) in a 1:1 weight ratio solution of 1,2-dimethoxyethane (DME) and 1,3-dioxolane (DOL) in an argon filled glove box. Lithium nitrate ($LiNO_3$) was used as additive in a concentration of 0.5 mol kg^{-1}. From here on, the electrolyte is named as DOLDME-LiTFSI-$LiNO_3$. DOL and DME solvents were dried under molecular sieves for several days before mixing, while the salts were dried under vacuum at 100°C for 24h. Before cells assembling, the as-prepared solution was stirred overnight. LTFSI, DME, DOL and $LiNO_3$ were acquired from Sigma Aldrich.

2.2 Active Materials and Electrode preparation

The sulfur-single-wall carbon nanohorns composite (S80SWCNH20) was prepared by an ease solvent evaporation method in order to infiltrate sulfur within the carbonaceous matrix. SWCNHs were provided by Advanced Technology Party (ATP) s.r.l., Italy. Elemental sulfur (from Sigma Aldrich) and SWCNHs were mixed in ethanol in a weight ratio of 80:20 and sonicated in a sonic bath for 2h. Afterward, the solvent was slowly evaporated at 60 °C under a pressure of 400 mbar. A schematic of the infiltration process is proposed in Figure 1.

Preprints (www.preprints.org) | NOT PEER-REVIEWED | Posted: 21 October 2022 doi:10.20944/preprints202210.0335.v1

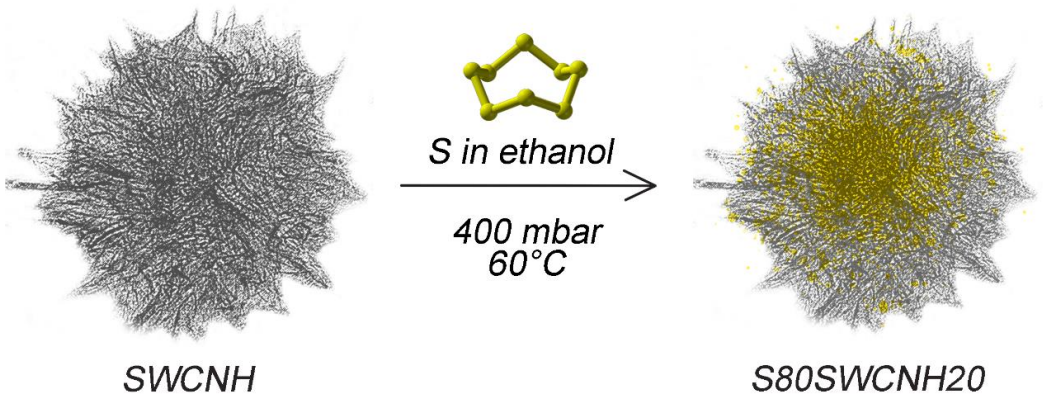

Figure 1 - Schematic illustration of the active material synthesis process.

The electrode slurry was prepared by mixing S80SWCNH20 active material, Super P carbon (from Imers) as conductive agent, and polyvinylidene difluoride (PVdF, from Solvay) as binder in 80:10:10 weight ratio using N-methylpyrrolidone NMP (from Sigma Aldrich) as solvent. The mixture was casted onto a carbon cloth current collector (AvCarb, from FuelCellStore) by employing the Doctor-Blade method and dried overnight at room temperature. The electrode foil was punched into 14 mm diameter disks, dried under vacuum at room temperature overnight and transferred in an argon-filled glovebox for cell assembly. The sulfur mass loading of the final electrodes was ~2 mg cm^{-2}.

2.3 Materials characterization

Thermogravimetric analysis (TGA) of the sulfur-SWCNHs composite was performed by using a Q500 thermogravimetric analyser from TA Instruments. The sample was heated up from 30 to 600°C at a 5°C min^{-1} heating rate under nitrogen flow. X-ray diffraction (XRD) patterns were collected using a Malvern PANalytical Empyrean instrument equipped with a Cu Kα source in the 2θ/θ scanning mode. Transmission electron microscopy (TEM), scanning transmission electron microscopy (STEM) and energy dispersive spectroscopy (STEM-EDS) images were acquired using a JOEL JEM-1400Plus equipped with a LaB_6 thermionic source operated at 120kV.

2.4 Electrochemical characterization

The electrochemical performance of S80SWCNH20 composite was tested in CR2032 coin cells, formed by lithium chips used as counter and reference electrode, a polymeric membrane (2400 Celgard) working as separator and the composite electrode S80SWCNH20 as electrode. Each cell was filled with 40 µl of DOLDME-LiTFSI-$LiNO_3$ electrolyte. The assembling process was carried out in an MBraun glovebox with water and oxygen levels lower than 0.1 ppm. The electrochemical characterization was performed by using a BCS-805 multichannel battery unit from BioLogic. Galvanostatic cycling tests of the sulfur-carbon electrode were performed at the current rates of C/4=420 mA g^{-1} in a 1.9 V-2.6 V voltage range and at 1C=1675 mA g^{-1} and 2C=3350 mA g^{-1} in a 1.6-2.8 V voltage range. Rate capability tests were carried out at different current rates, starting from C/10=167.5 mA g^{-1} up to 1C=1675 mA g^{-1} through C/8=210 mA g^{-1}, C/5=335 mA g^{-1}, C/2=837 mA g^{-1}, 1C=1675 mA g^{-1} and finally back to C/10.

Cyclic voltammetry tests were performed at the scan rate of 0.1 mV s^{-1} over a potential rage of 1.7-2.8 V. In order to evaluate the lithium ion diffusion coefficient (D_{cv}) within the cathode material, a cyclic voltammetry test was operated by increasing the scan rate (from 0.05 mV s^{-1} to 0.45 mV s^{-1}) in the above reported voltage range. D_{cv} of the S80SWCNH20s cathode was calculated through the Randles-Sevcik equation:[45]

$$I_p = 0.4463\, zFAC_{Li+}\sqrt{\frac{zF\nu D_{CV}}{RT}} \quad (1)$$

 doi:10.20944/preprints202210.0335.v1

where I_p is the peak current (A), z is the number of electrons exchanged in the oxidation/reduction process, F is the Faraday constant (C mol^{-1}), A is the active surface area of the electrode (cm^2), C_{Li+} is the lithium-ion concentration in the active material (mol cm^{-3}), ν is the voltage scan rate (V s^{-1}), R is the universal gas constant (J K^{-1} mol^{-1}), T is the employed temperature (K), with D_{cv} calculated in cm^2 s^{-1}.

Electrochemical impedance spectroscopy (EIS) measurements were carried out by applying a 10 mV AC amplitude signal in a frequency range of 1 MHz – 0.1 Hz. The impedance spectra were fitted by Boukamp software[46] by non-linear least squares fit (NLLSQ) and only the results with a chi-square (χ^2) lower than 10^{-4} were accepted. The equivalent circuit used to fit the data can be synthesized by the expression R_{el} $(RQ)_{SEI}$ $(R_{ct}Q_{dl})$ Q_{diff}, where R_{el} is the resistance of the electrolyte solution, $(RQ)_{SEI}$ is attributed to the formation of the solid electrolyte interface, R_{ct} refers to the charge transfer resistance, Q_{dl} is connected to the double layer capacitance ascribed to the lithiation and delithiation cathode reactions, and Q_{diff} is associated to the lithium ion diffusion into the electrode volume.

3. Results

3.1. Active material characterization

The S80SWCNH20 composite was prepared via simple evaporation method and employed as cathode active material in order to investigate its possible application in lithium-sulfur cells. The active material and the derived electrodes were analysed by addressing their chemical structure, morphology and electrochemical properties. The morphology of the pristine single-wall carbon nanohorns are shown in the TEM image of Figure 2(a). Three different types of nanohorns aggregates are present, namely bud-like, dahlia-like and seed-like structures, highlighted by coloured dashed circles. The SWCNHs diameter ranges from 50 to 150 nm. XRD analyses were carried out in order to confirm the presence and the crystalline phase of sulfur within the synthesized active material. Figure 2(b) reports the XRD spectra of pure SWCNHs and of the composite material together with the reference pattern of graphite and sulfur. The XRD spectrum of the SWCNHs reveals the presence of the characteristic peaks of graphite (ICCD: 00-058-1638, pink bars) where the peaks at 23° and about 43° can be attributed to the (002) and (10) reflections.[33] The pattern of the composite active material, in light blue, unveils the presence of the peaks attributed to orthorhombic sulfur (ICDD: 98-020-045, green bars) overlapped with the weaker SWCNHs broad peaks. In order to characterize the morphology of the composite sample after the synthesis and further verify the presence of sulfur within the SWCNHs, a STEM-EDS analysis was carried out and the results are reported in Figure 2(c). The dark-field TEM image of the S80SWCNH20 composite shows the three CNHs species, as also confirmed by the elemental mapping of carbon (pink), and highlights the absence of isolated sulfur aggregates. In this respect, the corresponding elemental mapping of sulfur (green) evidences the presence of a high sulfur concentration inside the carbon nanohorn structure. These observations suggest the presence of a morphology capable of encapsulating the dissolved LiPS species thus ameliorating the detrimental shuttle effect.[47,48]

Preprints (www.preprints.org) | NOT PEER-REVIEWED | Posted: 21 October 2022 doi:10.20944/preprints202210.0335.v1

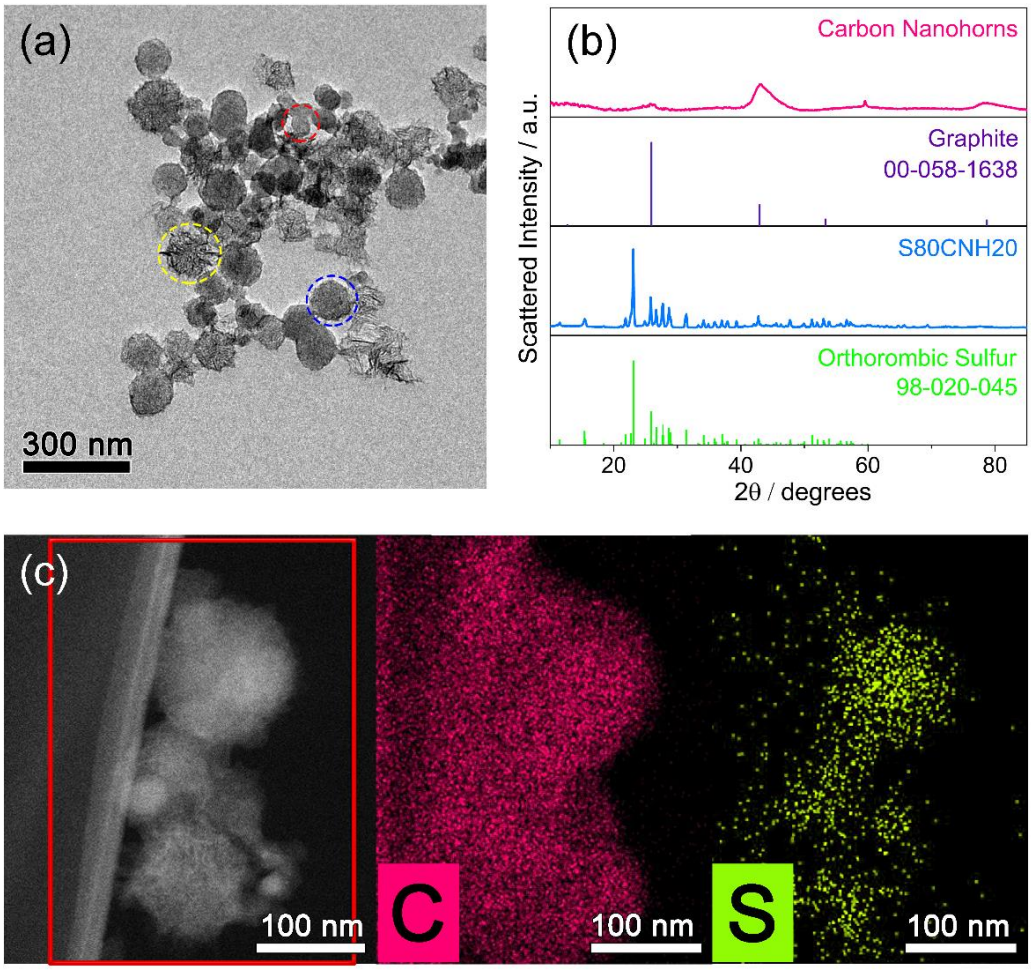

Figure 2 - (a) TEM image of single-walled carbon nanohorns: dahlia-like (yellow dashed circle), bud-like (blue dashed circle), and seed-like (red dashed circle) structures. (b) XRD spectrum of carbon nanohorns (pink line), reference pattern of graphite (ICCD: 00-058-1638, purple bars), sulfur-carbon nanohorns composite spectrum (light blue line) and reference pattern of orthorhombic sulfur (ICDD: 98-020-045, green bars). (c) TEM image and STEM-EDS maps of S80SWCNH20 active material.

The sulfur-carbon nanohorns composite was further investigated by TGA to find out its exact sulfur content. The measurement was carried out under argon in a 30-600 °C temperature range. Figure 3 shows the TGA profile, revealing an overall sulfur content of about 83% within the composite active material (66.4% of sulfur within the final electrode), while the remaining mass corresponds to the carbonaceous material. Thus, the simple evaporation method herein reported enabled the ease control of the sulfur and carbon amount. In the inset, the relative differential profile evidences a sulfur evaporation temperature of 230 °C.

Preprints (www.preprints.org) | NOT PEER-REVIEWED | Posted: 21 October 2022 doi:10.20944/preprints202210.0335.v1

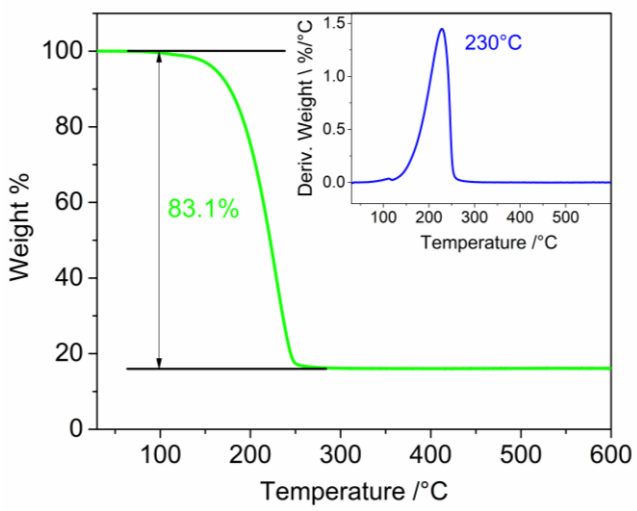

Figure 3 - TGA of the composite active material S80SWCNH20.

3.2. Electrochemical characterization

The electrochemical behaviour of the S80SWCNH20 composite electrode was explored using 2032 coin cells. DOLDME-LITFSI-$LiNO_3$ was employed as electrolytic solution in order to probe the performance of the electrode in lithium-sulfur batteries. Figure 4(a) reports the cyclic voltammetry curves (10 cycles) presenting the typical shape attributed to lithium-sulfur reactions within the selected electrolyte. Indeed, the cathodic scan shows a peak at 2.35 V is related to the conversion of S_8 rings to long-chain lithium polysulfide species Li_2S_x ($6 < x \leq 8$) while the second sharp peak at about 1.90 V suggests the reduction of the long-chain LiPSs to short-chain ones, i.e. Li_2S_x ($2 < x \leq 6$) and Li_2S.[49,50] Similarly, the anodic curve shows the first peak at ~ 2.35 V can be attributed to the oxidation of short chain LiPSs to high-order species, while the second peak at 2.45 V is related to the formation of long-chain polysulfide and finally of elemental sulfur.[51] The test evidences a decrease in the peaks intensity along the first five CV cycles, indicating a possible polysulfide dissolution within the electrolyte thus leading to active material loss.[52] After this initial intensity drop, the CV curves overlap one another, thus suggesting the cell stabilization upon cycling. EIS measurements were carried out before and after the CV test to investigate the internal resistance changes upon cycling. The associated Nyquist plot is reported in Figure 4(b). The impedance spectrum at the fresh state shows a broad and depressed semicircle with an overall resistance of 60 Ω which evolves into two semicircles after the CV test, revealing a total resistance of 15 Ω (see inset of Figure 4(b)). This value is indeed the combination of the electrolyte resistance (R_{el} = 3 Ω), the SEI resistance ($(RQ)_{SEI}$ = 5.5 Ω), and the charge transfer resistance (R_{ct} = 7.5 Ω). The first and the second semicircles can be ascribed to the formation of the solid electrolyte interphase (SEI) on the electrode surface and to the charge transfer processes occurring at the interface between electrode and electrolyte, respectively.[3] Indeed, the decrease of the cell resistance suggests the formation of a low resistive SEI facilitating the lithium ion transfer.[53]

Figure 4(c) reports the CV tests performed by increasing the scan rate from 0.05 to 0.45 mV s^{-1} in order to calculate D_{cv} within the electrode material (see Figure S1 of Supporting Information for EIS after each incremental step). As expected, by increasing the scan rate, the peak intensity increases accordingly due to the decreased size of the diffusion layer.[54] Moreover, increasing the scan rate determines a reduction of the cathodic peak potential and an increase of the anodic peak potential, a result due to mass transfer limitation.[55] D_{cv} was obtained through the Randles-Sevcik equation described in Eq. 1. This equation linearly correlates the peak current intensity (I_p) to the square root of the scan rate ($\nu^{1/2}$) (see Figure S2 of Supporting Information), where the slope value is dependent on the lithium diffusion coefficient.[56] D_{cv} was calculated for different states of charge

Preprints (www.preprints.org) | NOT PEER-REVIEWED | Posted: 21 October 2022 doi:10.20944/preprints202210.0335.v1

(2.35 and 2.45 V) and discharge (1.90 and 2.35 V) considering two electrons for each oxidation/reduction process. The results are reported in Figure 4(d) and, in details, the D_{cv} adds up to 2×10^{-10} and 1.6×10^{-10} cm^2 s^{-1} for the oxidation reaction occurring at 2.35 V and 2.45 V, respectively. Upon reduction, the lithium-ion diffusion appears to be slower for the reduction of S_8 to long-chain LiPSs at 2.35 V with respect to the reduction to short-chain LiPSs occurring at 1.90 V, showing D_{cv} values of about 5×10^{-11} and 2.2×10^{-10} cm^2 s^{-1}, respectively, in agreement with the CV test.

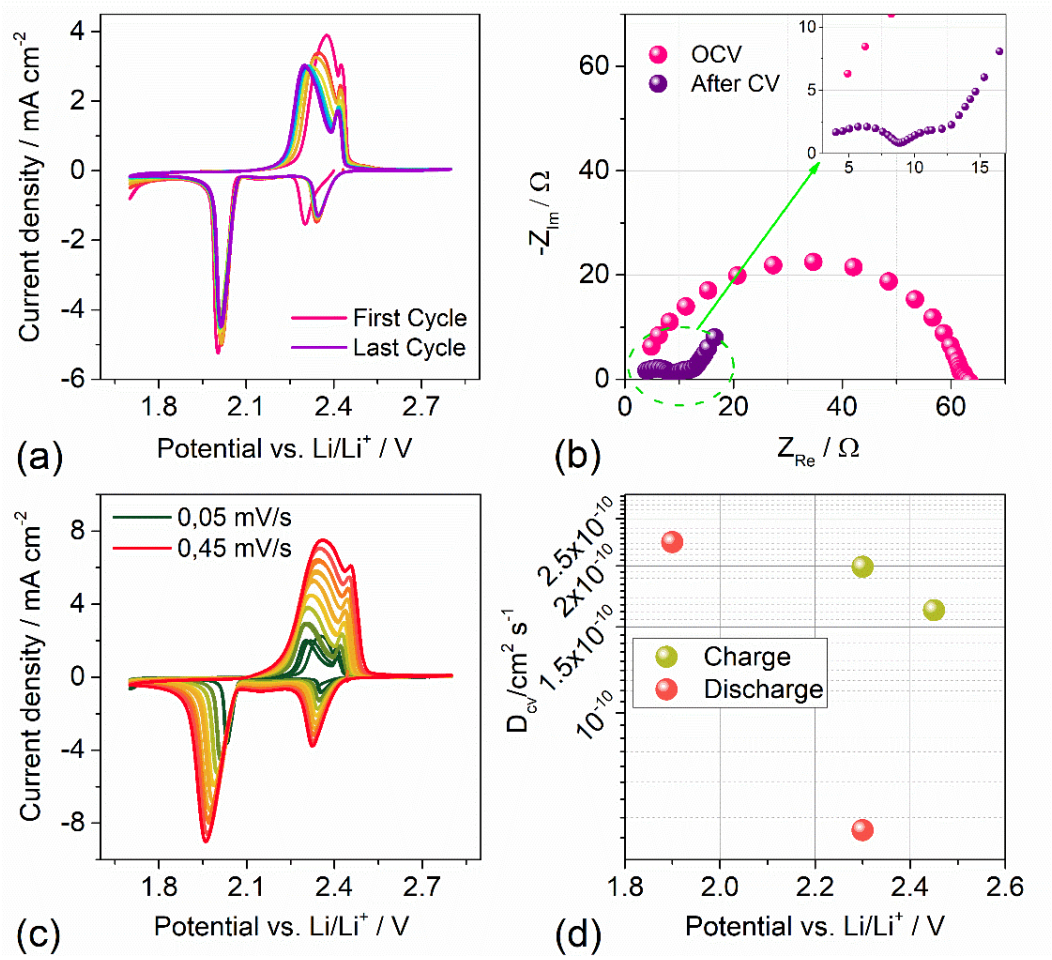

Figure 4 - (a) Cyclic voltammetry (CV) test of S80CNH20 electrode, performed in 2032-coin cell using DOLDME-LITFSI-LiNO3 as electrolyte in 1.7 V – 2.8 V voltage range with a scan rate of 0.1 mV s^{-1}. (b) EIS conducted as assembled and after the cyclic voltammetry. (c) CV tests carried out at increasing scan rate (from 0.05 to 0.45 mV s^{-1}) in order to calculate the lithium diffusion coefficient D_{cv} within the electrode material through Randles-Sevcik equation (see Eq. 1 and Figure S2 in the Supporting Information). (d) Lithium ion diffusion coefficients obtained by using the Randles–Sevcik equation, the peak intensity (I_P) and the scan rate (ν).

Rate capability and galvanostatic cycling tests were performed on the S80SWCNH20 electrode and are reported in Figure 5. In particular, Figures 5(a) and 5(b) display the rate capability tests performed by increasing the current rate from C/10 = 167.5 mA g^{-1} up to 1C = 1675 mA g^{-1} through C/8=210 mA g^{-1}, C/5=335 mA g^{-1}, C/2=837 mA g^{-1}, 1C=1675 mA g^{-1} and finally back to C/10 in a 1.6 V – 2.8 V voltage range. The tests were carried out to understand the cell behaviour at different current rates. As seen from Figure 5(a), the cell specific capacity decreases rapidly at C/10 during the first five cycles from 1135 down to 735 mA h g^{-1}, followed by a stabilization in the capacity values. By increasing the current rate, the cell polarization between charge and discharge curves increases from 0.2 V at C/10 to 0.4 V at 1C (Figure 5(b)) thus leading to a decrease in the cell specific capacity. Indeed, at 1C the delivered capacity is reduced to 570 mA h g^{-1}. Once the current is set

Preprints (www.preprints.org) | NOT PEER-REVIEWED | Posted: 21 October 2022 doi:10.20944/preprints202210.0335.v1

back to its original value (C/10), the cell recovers and maintains the specific capacity reached after the initial drop (~755 mA h g^{-1}). The initial fast capacity fading, well recognizable in Figure 5(a), can be ascribed to the presence of elemental sulfur on the carbon nanohorns surface, leading to the dissolution of LiPSs within the electrolyte and consequently to active material losses.[57] On the other hand, the subsequent stabilization in the specific capacity values could suggest LiPSs retention inside the SWCNHs, the latter acting as a physical barriers thus limiting the shuttle effect.[58] The voltage profiles (Figure 5(b)) show the characteristic curves attributed to the electrochemical reactions between lithium and sulfur. Indeed, two plateaus at 2.4 V and at 2.1 V during the discharge process are present, indicating the reduction of elemental sulfur to Li_2S discharge product. Upon charging, a long plateau is visible at 2.2 V, which increases up to 2.35 V along the test followed by a second short plateau at 2.4 V. The plots well highlight the cell polarization upon increasing the current rate. A prolonged galvanostatic cycling test was carried out at C/4 and it is reported in Figure 5(c). A similar behaviour to the rate capability test, with an initial capacity drop followed by a stabilization in the capacity values, is here observed. Indeed, the initial specific capacity of 656 mA h g^{-1} decreases down to 520 mA h g^{-1} in the first 10 cycles and remains stable for 400 cycles. Subsequently, the cell capacity slowly reduces reaching a value of about 300 mA h g^{-1} at the 775th cycle, which could be attributed to the formation of a 'dead sulfur' layer and an increase in the cell polarization, as it can be seen from the voltage profiles in Figure S3.[59] The coulombic efficiency of the S80SWCNH20 cell was maintained at about 96% throughout the whole test.

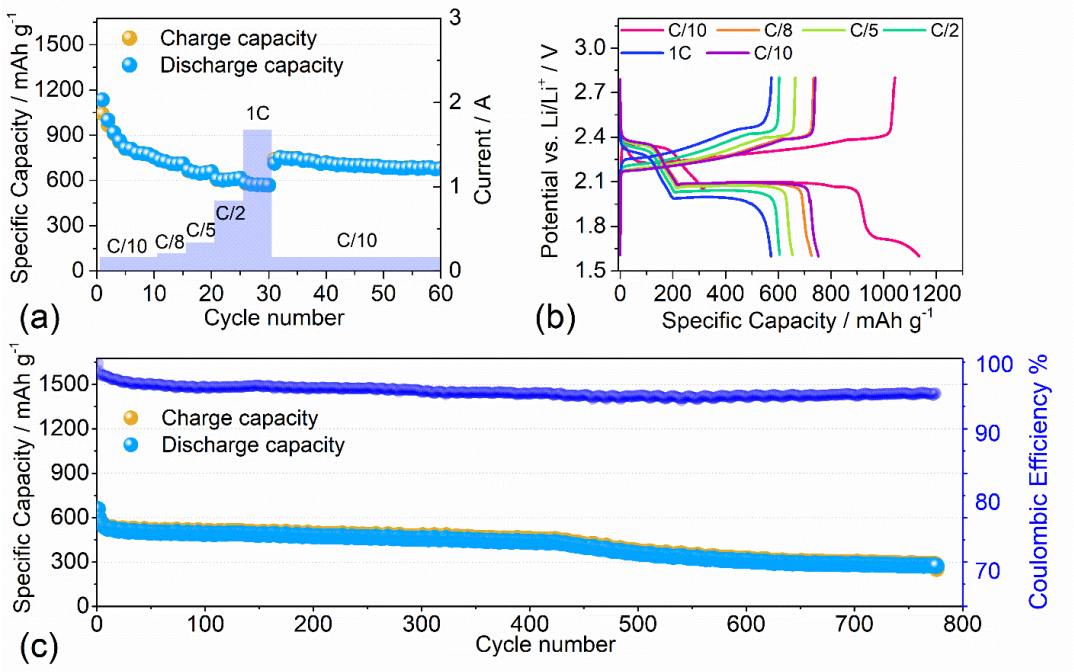

Figure 5 - (a) Rate capability test and (b) relative voltage profiles of S80CNH20 performed at different current-rate: C/10 to 1C (=1675 mA g^{-1}) through C/8, C/5, C/2 and 1C and finally back to C/10. Sulfur loading of ~2 mg cm^{-2}. (c) Galvanostatic cycling profile of the electrode performed in 2032-coin cells with DOLDME-LITFSI-$LiNO_3$ electrolyte carried out at C/4= 419 mA g^{-1} within 1.9 V and 2.6 V. Sulfur loading of ~2 mg cm^{-2} (see Figure S4 in SI for voltage profiles).

These results suggest the morphology as crucial parameter in order to stabilize the cell performance. Galvanostatic charge and discharge measurements were carried out on the S80SWCNH20 electrodes at the high current rate of 1C (1.675 A g^{-1}) and the results are reported in Figure S4 of Supporting Information. The test shows a high specific capacity if considering the high current rate, which could be ascribed to the high electronic conductivity of the carbon nanohorns combined with an optimized active material morphology.

 doi:10.20944/preprints202210.0335.v1

Overall, the S80SWCNH20 cells demonstrated a long cycle life without the addition of catalysts, functional materials nor the use of a complicated synthesis. The simple, ease and sustainable synthesis process herein employed to prepare the cell active material proved to be an effective way to produce a long cycle life sulfur-based electrode.

5. Conclusions

We have herein demonstrated a straightforward synthesis process to produce a sulfur-carbon nanohorns active material for next-generation lithium-sulfur batteries showing a long and stable cycle life. The facile and sustainable evaporation method reported in this work allows for the direct infiltration of elemental sulfur within single-walled carbon nanohorns. Moreover, the same synthesis process enables an ease control of the sulfur and carbon amount within the active material. In this respect, the active material was electrochemically tested in lithium-metal half-cells by employing a solution of bis(trifluoromethane)sulfonimide lithium salt and lithium nitrate in a mixture of 1,2-dimethoxyethane and 1,3-dioxolane. The obtained morphology enabled an important polysulfide retention by physically confining the soluble moieties within the SWCNH structures. Although a capacity drop is observed during the initial charge/discharge processes both at high and low current rates, the S80SWCNH20 cells demonstrated remarkable cycling performance, a result probably related to the presence of sulfur on the surface of the carbonaceous spheres. Indeed, at C/4 the cells showed a capacity of 520 mA h g^{-1} over 400 cycles thus reaching 300 mA h g^{-1} at the 775th cycle. A similar behaviour is encountered at 1C where, after the first 25 cycles, the cell exhibits a discharge capacity of about 600 mA h g^{-1} for 100 cycles.

Supplementary Materials: The following supporting information can be downloaded at: www.mdpi.com/xxx/s1, Figure S1: EIS of the S80SWCNH20 electrode acquired at each scan rate, from 0.05 to 0.45 mV s^{-1} along the cyclic voltammetry tests; Figure S2: Linear fit of the peak current (I_p) plotted vs. square root of the scan rate ($v^{1/2}$) of the cyclic voltammetry of Figure 4(c) of the S80SWCNH20 electrode for different states of charge; Figure S3: Voltage profiles of S80SWCNH20 performed at C/4 (= 419 mA g^{-1}) in a 1.7-2.8 V voltage range; Figure S4 : Galvanostatic cycling test of the S80SWNH20 electrode carried out at 1C (= 1675 mA g^{-1}).

Author Contributions: Conceptualization, E.V.; formal analysis, E.V.; investigation, E.V.; resources, R.P.Z.; data curation, E.V., P.S., S.C.; writing—original draft preparation, E.V.; writing—review and editing, R.P.Z., E.V., P.S., S.C.; supervision, R.P.Z.; project administration, E.V.; funding acquisition, R.P.Z. All authors have read and agreed to the published version of the manuscript.

Data Availability Statement: Not applicable.

Acknowledgments: We thank Dr. Rosaria Brescia and Luca Leoncino from the Electron Microscopy Facility at the Fondazione Istituto Italiano di Tecnologia for the STEM-EDX characterization. R.P.Z. wishes to recognize support from the Natural Science Foundation of China, grant no. 32071317.

Conflicts of Interest: The authors declare no conflict of interest.

References

1. Yuan, C.; Yang, X.; Zeng, P.; Mao, J.; Dai, K.; Zhang, L.; Sun, X. Recent Progress of Functional Separators with Catalytic Effects for High-Performance Lithium-Sulfur Batteries. *Nano Energy* **2021**, *84*, 105928, doi:10.1016/j.nanoen.2021.105928.
2. Larcher, D.; Tarascon, J.M. Towards Greener and More Sustainable Batteries for Electrical Energy Storage. *Nat. Chem.* **2015**, *7*, 19–29, doi:10.1038/nchem.2085.
3. Carbone, L.; Del Rio Castillo, A.E.; Kumar Panda, J.; Pugliese, G.; Scarpellini, A.; Bonaccorso, F.; Pellegrini, V. High-Sulfur-Content Graphene-Based Composite through Ethanol Evaporation for High-Energy Lithium-Sulfur Battery. *ChemSusChem* **2020**, *13*, 1593–1602, doi:10.1002/cssc.201902305.
4. Yang, X.; Li, X.; Adair, K.; Zhang, H.; Sun, X. Structural Design of Lithium–Sulfur Batteries: From Fundamental Research to Practical Application; *Springer Singapore*, **2018**; Vol. 1; ISBN 0123456789.
5. Younesi, R.; Veith, G.M.; Johansson, P.; Edström, K.; Vegge, T. Lithium Salts for Advanced Lithium Batteries: Li-Metal, Li-O2, and Li-S. *Energy Environ. Sci.* **2015**, *8*, 1905–1922, doi:10.1039/c5ee01215e.
6. Salama, M.; Rosy; Attias, R.; Yemini, R.; Gofer, Y.; Aurbach, D.; Noked, M. Metal-Sulfur Batteries: Overview and Research Methods. *ACS Energy Lett.* **2019**, *4*, 436–446, doi:10.1021/acsenergylett.8b02212.
7. Li, T.; Bai, X.; Gulzar, U.; Bai, Y.J.; Capiglia, C.; Deng, W.; Zhou, X.; Liu, Z.; Feng, Z.; Proietti Zaccaria, R. A Comprehensive Understanding of Lithium–Sulfur Battery Technology. *Adv. Funct. Mater.* **2019**, *29*, https://doi.org/10.1002/adfm.201901730.
8. Schön, P.; Krewer, U. Revealing the Complex Sulfur Reduction Mechanism Using Cyclic Voltammetry Simulation. *Electrochim. Acta* **2021**, *373*, https://doi.org/10.1016/j.electacta.2020.137523.
9. Wu, F.; Lee, J.T.; Fan, F.; Nitta, N.; Kim, H.; Zhu, T.; Yushin, G. A Hierarchical Particle-Shell Architecture for Long-Term Cycle Stability of Li<inf>2</Inf>S Cathodes. *Adv. Mater.* **2015**, *27*, 5579–5586, doi:10.1002/adma.201502289.
10. Benveniste, G.; Sánchez, A.; Rallo, H.; Corchero, C.; Amante, B. Comparative Life Cycle Assessment of Li-Sulphur and Li-Ion Batteries for Electric Vehicles. *Resour. Conserv. Recycl. Adv.* **2022**, *15*, 200086, doi:10.1016/j.rcradv.2022.200086.
11. Chung, S.H.; Chang, C.H.; Manthiram, A. A Core-Shell Electrode for Dynamically and Statically Stable Li-S Battery Chemistry. *Energy Environ. Sci.* **2016**, *9*, 3188–3200, doi:10.1039/c6ee01280a.
12. Knoop, J.E.; Ahn, S. Recent Advances in Nanomaterials for High-Performance Li – S Batteries. **2020**, *47*, 86–106, doi:10.1016/j.jechem.2019.11.018.
13. Urbonaite, S.; Poux, T.; Novák, P. Progress Towards Commercially Viable Li-S Battery Cells. *Adv. Energy Mater.* **2015**, *5*, 1–20, doi:10.1002/aenm.201500118.
14. Fan, X.; Sun, W.; Meng, F.; Xing, A.; Liu, J. Advanced Chemical Strategies for Lithium–Sulfur Batteries: A Review. *Green Energy Environ.* **2018**, *3*, 2–19, doi:10.1016/j.gee.2017.08.002.
15. He, Q.; Gorlin, Y.; Patel, M.U.M.; Gasteiger, H.A.; Lu, Y.-C. Unraveling the Correlation between Solvent Properties and Sulfur Redox Behavior in Lithium-Sulfur Batteries. *J. Electrochem. Soc.* **2018**, *165*, A4027–A4033, doi:10.1149/2.0991816jes.
16. Liu, J.; Chen, H.; Chen, W.; Zhang, Y.; Zheng, Y. New Insight into the "Shuttle Mechanism" of Rechargeable Lithium-Sulfur Batteries. *ChemElectroChem* **2019**, *6*, 2782–2787, https://doi.org/10.1002/celc.201900420.
17. Liang, X.; Kwok, C.Y.; Lodi-Marzano, F.; Pang, Q.; Cuisinier, M.; Huang, H.; Hart, C.J.; Houtarde, D.; Kaup, K.; Sommer, H.; et al. Tuning Transition Metal Oxide-Sulfur Interactions for Long Life Lithium Sulfur Batteries: The "Goldilocks" Principle. *Adv. Energy Mater.* **2016**, *6*, 1–9, doi:10.1002/aenm.201501636.
18. Hwang, J.Y.; Kim, H.M.; Lee, S.K.; Lee, J.H.; Abouimrane, A.; Khaleel, M.A.; Belharouak, I.; Manthiram, A.; Sun, Y.K. High-Energy, High-Rate, Lithium-Sulfur Batteries: Synergetic Effect of Hollow TiO2-Webbed Carbon Nanotubes and a Dual Functional Carbon-Paper Interlayer. *Adv. Energy Mater.* **2016**, *6*, doi:10.1002/aenm.201501480.
19. Liu, Y.; Qin, X.; Zhang, S.; Liang, G.; Kang, F.; Chen, G.; Li, B. Fe3O4-Decorated Porous Graphene Interlayer for High-Performance Lithium-Sulfur Batteries. *ACS Appl. Mater. Interfaces* **2018**, *10*, 26264–26273, doi:10.1021/acsami.8b07316.
20. Gupta, A.; Bhargav, A.; Manthiram, A. Highly Solvating Electrolytes for Lithium–Sulfur Batteries. *Adv. Energy Mater.* **2019**, *9*, 1–9, doi:10.1002/aenm.201803096.

21. McOwen, D.W.; Seo, D.M.; Borodin, O.; Vatamanu, J.; Boyle, P.D.; Henderson, W.A. Concentrated Electrolytes: Decrypting Electrolyte Properties and Reassessing Al Corrosion Mechanisms. *Energy Environ. Sci.* **2014**, *7*, 416–426, doi:10.1039/c3ee42351d.
22. Cho, S.H.; Cho, S.M.; Bae, K.Y.; Kim, B.H.; Son, B.D.; Yoon, W.Y. Improving Electrochemical Properties of Lithium–Sulfur Batteries by Adding a Catalyst-Embedded Interlayer. *Electrochim. Acta* **2019**, *315*, 33–40, doi:10.1016/j.electacta.2019.05.062.
23. Hwa, Y.; Cairns, E.J. Nanostructured Sulfur and Sulfides for Advanced Lithium/Sulfur Cells. *ChemElectroChem* **2020**, *7*, 3927–3942, doi: 10.1002/celc.202000758.
24. Weret, M.A.; Su, W.N.; Hwang, B.J. Strategies towards High Performance Lithium-Sulfur Batteries. *Batter. Supercaps* **2022,** *5*, doi: 10.1002/batt.202200059.
25. Fan, K.; Huang, H. Two-Dimensional Host Materials for Lithium-Sulfur Batteries: A Review and Perspective. *Energy Storage Mater.* **2022**, *50*, 696–717, doi:10.1016/j.ensm.2022.06.009.
26. Liang, X.; Nazar, L.F. In Situ Reactive Assembly of Scalable Core-Shell Sulfur-MnO2 Composite Cathodes. *ACS Nano* **2016**, *10*, 4192–4198, doi:10.1021/acsnano.5b07458.
27. Doñoro, Á.; Muñoz-Mauricio, Á.; Etacheri, V. High-Performance Lithium Sulfur Batteries Based on Multidimensional Graphene-CNT-Nanosulfur Hybrid Cathodes. *Batteries* **2021**, *7*, doi: 10.3390/batteries7020026.
28. Ma, Z.; Jing, F.; Fan, Y.; Li, J.; Zhao, Y.; Shao, G. High Electrical Conductivity of 3D Mesporous Carbon Nanocage as an Efficient Polysulfide Buffer Layer for High Sulfur Utilization in Lithium-Sulfur Batteries. *J. Alloys Compd.* **2019**, *789*, 71–79, doi:10.1016/j.jallcom.2019.03.035.
29. Laverde, J.; Rosero-Navarro, N.C.; Miura, A.; Buitrago-Sierra, R.; Tadanaga, K.; López, D. Impact of Sulfur Infiltration Time and Its Content in an N-Doped Mesoporous Carbon for Application in Li-S Batteries. *Batteries* **2022**, *8*, 58. doi: 10.3390/batteries8060058
30. Kang, H.J.; Rafiqul Bari, G.A.K.M.; Lee, T.G.; Khan, T.T.; Park, J.W.; Hwang, H.J.; Cho, S.Y.; Jun, Y.S. Microporous Carbon Nanoparticles for Lithium-Sulfur Batteries. *Nanomaterials* **2020**, *10*, 1–17, doi:10.3390/nano10102012.
31. Zhou, K.; Fan, X.J.; Wei, X.F.; Liu, J.H. The Strategies of Advanced Cathode Composites for Lithium-Sulfur Batteries. *Sci. China Technol. Sci.* **2017**, *60*, 175–185, doi:10.1007/s11431-016-0664-0.
32. Rajkumar, P.; Diwakar, K.; Subadevi, R.; Gnanamuthu, R.M.; Sivakumar, M. Sulfur Cloaked with Different Carbonaceous Materials for High Performance Lithium Sulfur Batteries. *Curr. Appl. Phys.* **2019**, *19*, 902–909, doi:10.1016/j.cap.2019.05.001.
33. Bandow, S.; Kokai, F.; Takahashi, K.; Yudasaka, M.; Qin, L.C.; Iijima, S. Interlayer Spacing Anomaly of Single-Wall Carbon Nanohorn Aggregate. *Chem. Phys. Lett.* **2000**, *321*, 514–519, doi:10.1016/S0009-2614(00)00353-5.
34. Kasuya, D.; Yudasaka, M.; Takahashi, K.; Kokai, F.; Iijima, S. Selective Production of Single-Wall Carbon Nanohorn Aggregates and Their Formation Mechanism. *J. Phys. Chem. B* **2002**, *106*, 4947–4951, doi:10.1021/jp020387n.
35. Li, N.; Wang, Z.; Zhao, K.; Shi, Z.; Gu, Z.; Xu, S. Synthesis of Single-Wall Carbon Nanohorns by Arc-Discharge in Air and Their Formation Mechanism. *Carbon N. Y.* **2010**, *48*, 1580–1585, doi:10.1016/j.carbon.2009.12.055.
36. Iijima, S.; Yudasaka, M. Nano-Aggregates of Single-Walled Graphitic Carbon Nano-Horns. **1999**, *309*, 165–170, doi:10.1016/S0009-2614(99)00642-9.
37. Takikawa, H.; Ikeda, M.; Hirahara, K.; Hibi, Y.; Tao, Y.; Ruiz, P.A.; Sakakibara, T.; Itoh, S.; Iijima, S. Fabrication of Single-Walled Carbon Nanotubes and Nanohorns by Means of a Torch Arc in Open Air. *Phys. B Condens. Matter* **2002**, *323*, 277–279, doi:10.1016/S0921-4526(02)00998-5.
38. Wu, W.; Zhao, Y.; Wu, C.; Guan, L. Single-Walled Carbon Nanohorns with Unique Horn-Shaped Structures as a Scaffold for Lithium-Sulfur Batteries. *RSC Adv.* **2014**, *4*, 28636–28639, doi:10.1039/c4ra03693j.
39. Gulzar, U.; Li, T.; Bai, X.; Colombo, M.; Ansaldo, A.; Marras, S.; Prato, M.; Goriparti, S.; Capiglia, C.; Proietti Zaccaria, R. Nitrogen-Doped Single-Walled Carbon Nanohorns as a Cost-Effective Carbon Host toward High-Performance Lithium-Sulfur Batteries. *ACS Appl. Mater. Interfaces* **2018**, *10*, 5551–5559, doi:10.1021/acsami.7b17602.
40. Zhao, Y.; Li, J.; Ding, Y.; Guan, L. Single-Walled Carbon Nanohorns Coated with Fe2O3 as a Superior Anode Material for

Lithium Ion Batteries. *Chem. Commun.* **2011**, *47*, 7416–7418, doi: 10.1039/C1CC12171E.

41. Wang, J.; Hu, Z.; Xu, J.; Zhao, Y. Therapeutic Applications of Low-Toxicity Spherical Nanocarbon Materials. *NPG Asia Mater.* **2014**, *6*, doi: 10.1038/am.2013.79.
42. Zhu, S.; Xu, G. Single-Walled Carbon Nanohorns and Their Applications. *Nanoscale* **2010**, *2*, 2538–2549, doi:10.1039/c0nr00387e.
43. Nan, Y.; He, Y.; Zhang, Z.; Wei, J.; Zhang, Y. Controllable Synthesis of N-Doped Carbon Nanohorns: Tip from Closed to Half-Closed, Used as Efficient Electrocatalysts for Oxygen Evolution Reaction. *RSC Adv.* **2021**, *11*, 35463–35471, doi:10.1039/d1ra06458d.
44. Zhang, Z.; Han, S.; Wang, C.; Li, J.; Xu, G. Single-Walled Carbon Nanohorns for Energy Applications. *Nanomaterials* **2015**, *5*, 1732–1755, doi:10.3390/nano5041732.
45. Kim, T.; Choi, W.; Shin, H.C.; Choi, J.Y.; Kim, J.M.; Park, M.S.; Yoon, W.S. Applications of Voltammetry in Lithium Ion Battery Research. *J. Electrochem. Sci. Technol.* **2020**, *11*, 14–25, doi:10.33961/jecst.2019.00619.
46. BOUKAMP, B. A Nonlinear Least Squares Fit Procedure for Analysis of Immittance Data of Electrochemical Systems. *Solid State Ionics* **1986**, *20*, 31–44, doi:10.1016/0167-2738(86)90031-7.
47. Pan, J.; Sun, Y.; Wu, Y.; Li, J.; Huang, W.; Shi, K.; Lin, Y.; Dong, H.; Liu, Q. Yolk-Double Shells Hierarchical N-Doped Carbon Nanosphere as an Electrochemical Nanoreactor for High Performance Lithium-Sulfur Batteries. *Carbon N. Y.* **2022**, *198*, 80–90, doi:10.1016/j.carbon.2022.06.073.
48. Li, H.; Sun, L.; Wang, Z.; Zhang, Y.; Tan, T.; Wang, G.; Bakenov, Z. Three-Dimensionally Hierarchical Graphene Based Aerogel Encapsulated Sulfur as Cathode for Lithium/Sulfur Batteries. *Nanomaterials* **2018**, *8*, 1–12, doi:10.3390/nano8020069.
49. Chung, S.H.; Chang, C.H.; Manthiram, A. A Core-Shell Electrode for Dynamically and Statically Stable Li-S Battery Chemistry. *Energy Environ. Sci.* **2016**, *9*, 3188–3200, doi:10.1039/c6ee01280a.
50. Gorlin, Y.; Patel, M.U.M.; Freiberg, A.; He, Q.; Piana, M.; Tromp, M.; Gasteiger, H.A. Understanding the Charging Mechanism of Lithium-Sulfur Batteries Using Spatially Resolved Operando X-Ray Absorption Spectroscopy. *J. Electrochem. Soc.* **2016**, *163*, A930–A939, doi:10.1149/2.0631606jes.
51. Ng, S.F.; Lau, M.Y.L.; Ong, W.J. Lithium–Sulfur Battery Cathode Design: Tailoring Metal-Based Nanostructures for Robust Polysulfide Adsorption and Catalytic Conversion. *Adv. Mater.* **2021**, doi:10.1002/adma.202008654.
52. Kaiser, M.R.; Han, Z.; Liang, J.; Dou, S.X.; Wang, J. Lithium Sulfide-Based Cathode for Lithium-Ion/Sulfur Battery: Recent Progress and Challenges. *Energy Storage Mater.* **2019**, *19*, 1–15, doi:10.1016/j.ensm.2019.04.001.
53. Krauss, F.T.; Pantenburg, I.; Roling, B. Transport of Ions, Molecules, and Electrons across the Solid Electrolyte Interphase: What Is Our Current Level of Understanding? *Adv. Mater. Interfaces* **2022**, *9*, doi: 10.1002/admi.202101891.
54. Elgrishi, N.; Rountree, K.J.; McCarthy, B.D.; Rountree, E.S.; Eisenhart, T.T.; Dempsey, J.L. A Practical Beginner's Guide to Cyclic Voltammetry. *J. Chem. Educ.* **2018**, *95*, 197–206, doi:10.1021/acs.jchemed.7b00361.
55. Espinoza, E.M.; Clark, J.A.; Soliman, J.; Derr, J.B.; Morales, M.; Vullev, V.I. Practical Aspects of Cyclic Voltammetry: How to Estimate Reduction Potentials When Irreversibility Prevails. *J. Electrochem. Soc.* **2019**, *166*, H3175–H3187, doi: 10.1149/2.0241905jes.
56. Di Lecce, D.; Brescia, R.; Scarpellini, A.; Prato, M.; Hassoun, J. A High Voltage Olivine Cathode for Application in Lithium-Ion Batteries. *ChemSusChem* **2016**, *9*, 223–230, doi:10.1002/cssc.201501330.
57. Huang, X.; Luo, B.; Knibbe, R.; Hu, H.; Lyu, M.; Xiao, M.; Sun, D.; Wang, S.; Wang, L. An Integrated Strategy towards Enhanced Performance of the Lithium–Sulfur Battery and Its Fading Mechanism. *Chem. - A Eur. J.* **2018**, *24*, 18544–18550, doi:10.1002/chem.201804369.
58. Pozio, A.; Di Carli, M.; Aurora, A.; Falconieri, M.; Seta, L. Della; Prosini, P.P. Hard Carbons for Use as Electrodes in Li-S and Li-Ion Batteries. *Nanomaterials* **2022**, *12*, doi:10.3390/nano12081349.
59. Zhao, M.; Chen, X.; Li, X.Y.; Li, B.Q.; Huang, J.Q. An Organodiselenide Comediator to Facilitate Sulfur Redox Kinetics in Lithium–Sulfur Batteries. *Adv. Mater.* **2021**, *33*, doi: 10.1002/adma.202007298.